Funct Integr Genomics (2012) 12:119–130
DOI 10.1007/s10142-012-0263-6

ORIGINAL PAPER

Genome-wide ChIP-seq mapping and analysis reveal butyrate-induced acetylation of H3K9 and H3K27 correlated with transcription activity in bovine cells

Joo Heon Shin · Robert W. Li · Yuan Gao · Ransom Baldwin VI · Cong-jun Li

Received: 28 September 2011 / Revised: 29 December 2011 / Accepted: 2 January 2012 / Published online: 17 January 2012

Abstract Butyrate-induced histone acetylation plays an important role in the regulation of gene expression. However, the regulation mechanisms of histone modification remain largely unclear. To comprehensively analyze histone modification induced by butyrate, we utilized chromatin immunoprecipitation (ChIP) technology combined with next-generation sequencing technology (ChIP-seq) to analyze histone modification (acetylation) induced by butyrate and to map the epigenomic landscape of normal histone H3 and acetylated histone H3K9 and H3K27 on a large scale. To determine the location of histone H3, acetyl-H3K9, and acetyl-H3K27 binding sites within the bovine genome, we analyzed the H3-, acetyl-H3K9-, and acetyl-H3K27-enriched binding regions in the proximal promoter within 5 kb upstream, or at the 5′ untranslated region (UTR) from the transcriptional start site (TSS), exon, intron, and intergenic regions (defined as regions 25 kb upstream or 10 kb downstream from the TSS). Our analysis indicated that the distribution of histone H3, acetyl-H3K9, and acetyl-H3K27 correlated with transcription activity induced by butyrate. Using the GADEM algorithm, several motifs were generated for each of the ChIP-seq datasets. A de novo search for H3, acetyl-H3K9, and acetyl-H3K27 binding motifs indicated that histone modification (acetylation) at various locations changes the histone H3 binding preferences. Our results reveal that butyrate-induced acetylation in H3K9 and H3K27 changes the sequence-based binding preference of histone H3 and underlies the potential mechanisms of gene expression regulation induced by butyrate.

Keywords Bovine · Butyrate · ChIP-seq · Epigenomics · Histone acetylation

Mention of a product, reagent, or source does not constitute an endorsement by the USDA to the exclusion of other products or services that perform a comparable function.

Electronic supplementary material The online version of this article (doi:10.1007/s10142-012-0263-6) contains supplementary material, which is available to authorized users.

J. H. Shin · Y. Gao
Lieber Institute for Brain Development, Johns Hopkins University,
855 North Wolfe Street, Suite 102,
Baltimore, MD 21205, USA

R. W. Li · R. Baldwin VI · C.-j. Li (✉)
Bovine Functional Genomics Laboratory,
Animal and Natural Resources Institute, ARS, USDA,
10300 Baltimore Ave, Building 200, Room 209, BARC East,
Beltsville, MD 20705, USA
e-mail: congjun.li@ars.usda.gov

Introduction

Beyond their nutritional importance, volatile short-chain fatty acids (VFAs; acetate, propionate, and butyrate), especially butyrate, modulate cell differentiation, proliferation, and motility, and also induce cell cycle arrest and apoptosis. Most previous studies have focused on the therapeutic potential of butyrate for cancer, and thus have used cancer cell lines as research models (Myzak and Dashwood 2006). The cell cycle regulatory effects of butyrate at the cellular and molecular levels in normal bovine cells have not been studied until recently (Li and Elsasser 2005; Li and Li 2006, 2007). The principle biochemical change in cells treated with butyrate and other histone deacetylase (HDAC) inhibitors is the global hyperacetylation of histones (Riggs et al. 1977; Li and Elsasser 2005; Li et al. 2010). Clear evidence links modifications in chromatin structure to cell cycle progression, DNA replication, and overall chromosome stability (Wolffe and Guschin 2000). However, the molecular basis for these effects on the cell cycle is still poorly defined.

The modulation of genome expression as a consequence of chromatin structural changes is likely a mechanism with a major role in determining tissue responses. Data from in vitro experiments on bovine cells (MDBK) show that as a direct result of the hyperacetylation of histones induced by butyrate treatment at physiological concentrations (2.5–10 mM), cultured bovine cells are arrested in the early G1 phase and DNA synthesis is eliminated, as assayed by BrdU incorporation and flow cytometric analyses (Li and Elsasser 2005). At a relatively high concentration (10 mM), butyrate also induces apoptosis in an established bovine MDBK cell line (Li and Elsasser 2005). In primary cultures of isolated ruminal epithelial cells, DNA replication is also inhibited by butyrate treatment (Baldwin 1999). In addition, butyrate may also alter histone methylation as a histone deacetylase inhibitor (Marinova et al. 2010), suggesting an interplay between histone acetylation and methylation.

An investigation of global gene expression profiles of bovine kidney epithelial cells, regulated by sodium butyrate using high-density oligonucleotide microarray was completed recently (Li and Li 2006; Li et al. 2007), determining that as much as 8% of genes are regulated by butyrate. We identified 450 genes that were significantly regulated by sodium butyrate at a very stringent false discovery rate (FDR) of 0%. The functional category and pathway analyses of the microarray data revealed that four canonical pathways (cell cycles: G2/M DNA damage checkpoint, pyrimidine metabolism, G1/S checkpoint regulation, and purine metabolism) were significantly perturbed. Moreover, the biologically relevant networks and pathways of these genes were also identified. They included genes such as *IGF2*, *TGFB1*, *TP53*, *E2F4*, and *CDC2*, which were established as central to these networks. Taken together, these studies demonstrate that butyrate exerts an effect on genes associated with regulatory pathways critical to cell growth, immune response, and signal transduction (Li and Li 2006; Fischer et al. 2007). The profound changes in gene expression elucidate the pleiotropic effects of histone acetylation induced by butyrate in bovine cells. A majority of these genes were repressed by butyrate and tend to be associated with cell cycle control. Following our report of butyrate's biological effects on bovine cells, it was found that butyrate can also greatly enhance the derivation of human pluripotent stem cells by promoting epigenetic remodeling and the expression of pluripotency-associated genes (Mali et al. 2010).

The HDAC inhibition activity of butyrate makes it a great inducer of the hyperacetylation of histone in cells. Discovering the extent to which the epigenomic landscape is modified by butyrate-induced histone acetylation is a critical step in the path to understanding how this nutrient affecting specific transcriptome changes at the mechanistic level. We report here the first comprehensive approach to the investigation of epigenetic changes correlated with butyrate treatment in bovine cells. We demonstrate the functional characterization of butyrate-induced histone modification by profiling H3 core, butyrate-induced acetyl-H3K9, and acetyl-H3K27 in MDBK cells using ChIP-seq technology and assessing or mapping the "epigenomic code/landscape." Our results reveal that butyrate-induced acetylation of H3K9 and H3K27 changes the sequence-based binding preference of histone H3 and underlies the potential mechanisms of gene expression regulation induced by butyrate.

Materials and methods

Cell culture and butyrate treatments

The Madin–Darby bovine kidney epithelial cells (MDBK; American Type Culture Collection, Manassas, VA; Catalog No. CCL-22) were cultured in Eagle's minimal essential medium and supplemented with 5% fetal bovine serum (Invitrogen, Carlsbad, CA) in 25-cm^2 flasks, as described in our previous report (Li and Elsasser 2005). At approximately 50% confluence, the cells were treated with 10 mM of sodium butyrate for 24 h during the exponential phase (Calbiochem, San Diego, CA). A butyrate concentration of 10 mM was selected, as it represents a physiologically relevant dose and has previously been successfully used to evoke desired changes in cell cycle dynamics (Li and Elsasser 2005). Three replicate flasks of cells for both treatment and control groups (six samples in total) were used for the ChIP experiments.

ChIP

A ChIP-IT™ Express Enzymatic Kit (Active Motif North America, Carlsbad, CA) was used for this ChIP experiment. Antibodies against H3 (category #2650, cross-react to cow H3, ChIP formulated, Cell Signaling Technology), acetyl-H3K9 (ab10812, ChIP grade, us.orders@abcam.com), and acetyl-H3K27 (ab4729, ChIP grade, us.orders@abcam.com) were obtained from Abcam. The anti-H3 core, acetyl-H3K9, and acetyl-H3K27 antibodies were characterized and validated for cross-reactivity before the ChIP experiments with Western blots and immunoprecipitation (IP). The preparation of sheared chromatin (cell fixation, enzymatic shearing) was performed per the product manufacturer's instructions. Briefly, cells were fixed with 1% formaldehyde in flasks at room temperature for 10 min and subsequently washed with ice-cold PBS before a 0.1-M glycine solution was added to stop the fixation. The cells were scraped from the flask and homogenized with an ice-cold Dounce homogenizer to release the nuclei. The collected nuclei were resuspended in a digestion buffer, and an enzymatic shearing cocktail was added and incubated for

20 min at 37°C. The shearing reaction was stopped by adding 10 μl of ice-cold 0.5 M EDTA prior to centrifugation at 15,000 rpm in a 4°C microcentrifuge. The supernatant containing the sheared chromatin was carefully collected and prepared for ChIP sequencing. Next, 10 μg of primary antibody was added to 100 μl of chromatin and incubated on an end-to-end rotator overnight at 4°C. Subsequently, 50 μl of protein G magnetic beads were added, and incubation continued for another 4 h. The magnetic beads were washed with a ChIP buffer 1 once and a ChIP buffer 2 twice before the bound chromatin was eluted, and cross-links were reversed and treated with protease K.

Next-generation sequencing

All standard protocols for Illumina sequence preparation, sequencing, and quality control are provided by Illumina. In short, DNA recovered from a conventional ChIP procedure was quantified using the QuantiFluor fluorometer (Promega, Madison, WI). The DNA integrity was verified using the Agilent Bioanalyzer 2100 (Agilent; Palo Alto, CA, USA). The DNA was then processed, including end repair, adaptor ligation, and size selection, using an Illumina sample prep kit following the manufacturer's instructions (Illumina, San Diego, CA, USA). Final DNA libraries were validated and sequenced at 75 bp per sequence read, using an Illumina GAIIx sequencer at a depth of approximately 30 million sequences per sample (mean±SD=28±4 million per sample).

ChIP-seq analysis

Sequencing tags were aligned to the bosTau4 Oct 2007 release of the reference genome using Bowtie, an ultrafast memory-efficient short read aligner (Langmead et al. 2009a). We considered those tags that aligned uniquely with less than two mismatches. For enriched-region (peak) identification (peak calling), we used the Model-based Analysis of ChIP-seq (MACS) algorithm (Zhang et al. 2008; Feng et al. 2011). A simple yet effective technique for the analysis of eukaryotes, MACS was designed to identify transcription factor binding sites and histone modification-enriched regions in ChIP-seq data sets, with or without control samples. The application of the ChIP-seq facilitated the identification of binding sites associated with transcription factors and regions of histone modification. The MEME 4.6.1 (Bailey and Elkan 1994) was used for motif discovery. The PeakAnalyzer (Salmon-Divon et al. 2010) was used for peak annotation, nearest downstream gene (NDG) analysis, and transcriptional start site (TSS) analysis. The overall processing procedure is summarized in Supplementary Fig. 1.

Results

ChIP-seq

We first validated the reliability of the three antibodies (antibodies against histone H3, acetyl-H3K9, and acetyl-H3K27) we are using for the ChIP experiment. Figure 1 shows that all three antibodies have cross-reactivity to bovine histone H3, acetyl-H3K9, and acetyl-H3K27. The antibody against histone H3 detected H3 in cell lyses from MDBK cells with or without butyrate treatment, while antibodies against acetyl-H3K9 and acetyl-H3K27 react strongly to butyrate-induced accumulations of acetyl H3K9 and acetyl-H3K27. All three antibodies also work very well in immunoprecipitation experiments to precipitate H3, acetyl-H3K9, and acetyl-H3K27, respectively.

Using these antibodies, we performed a ChIP-seq on three samples: total histone H3 from normal growing cells, histone H3 lysine 9 acetylation (acetyl-H3K9), and histone H3 lysine 27 acetylation (acetyl-H3K27) from butyrate-treated cells. A normal H3 ChIP served as a positive control as well as a baseline for acetylated histone. We used BOWTIE, an ultrafast memory-efficient short read aligner (Langmead et al. 2009b), to align sequencing reads to the reference genome (bosTau4), and the alignment results are presented in Table 1. All three ChIP-seq data aligned well with the reference genome. This process resulted in a total of more than 84,000,000 reads and nearly 768,000,000 (~91%) aligned reads, covering ~4,800,000,000 bases of the bovine genome.

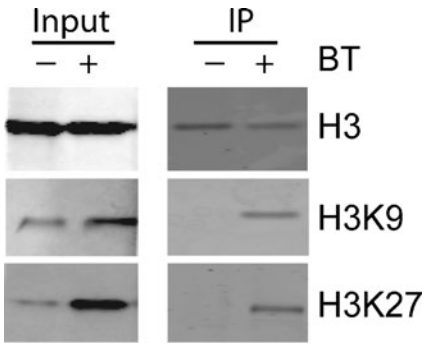

Fig. 1 Validation of antibodies: cells with or without butyrate treatment were extracted with an M-Per buffer (Mammalian Protein Extraction Reagent, Pierce Biotechnology) plus 250 mM of NaCl. Aliquots of the cell extracts were either mixed with SDS sample buffer (input), or were first immuneprecipitated with H3, acetyl-H3K9, or acetyl-H3K27 antibodies, respectively. For IP, 1.0 μg of primary antibody was added to 100 μl of cell extracts and incubated on an end-to-end rotator overnight at 4°C. Subsequently, 10 μl of protein A/G magnetic beads were added, and incubation continued for another 4 h. The magnetic beads were washed with ChIP buffer 1 once and ChIP buffer 2 twice before the bound chromatin was eluted with SDS sample buffer (*IP*). Input and IP samples were separated by SDS-PAGE and transferred to nitrocellulose membrane. Western blot analyses were performed using anti H3, acetyl-H3K9, and acetyl-H3K27

Table 1 ChIP-seq and alignment results

	H3	Acetyl-H3K9	Acetyl-H3K27
Total reads	2,978,0699	23,326,139	30,901,336
Aligned reads	27,078,053	21,368,435	28,318,383
% Aligned	90.92	91.61	91.64

ChIP-seq analysis

We used MACS version 1.4 (Orc2, 20110214) for enriched-region (peak) identification, with the arguments set as follows: bandwidth=200, model fold=10, 30, *P* value cutoff=1.00e−05. The range for calculating the regional lambda was 10,000 bps. The ChIP-seq for the anti-H3 sample generated 16,927 enriched regions, whereas the ChIP-seq for the anti-acetyl-H2K9 sample generated 9,160 enriched regions and the anti-H3K27 sample generated 50,754 enriched regions, respectively.

Genome-wide distributions of histone H3 in normal bovine cells and acetyl-histone H3 (H3K9 and H3K27) in butyrate-treated cells

The peak distribution of the ChIP-seq reads of normal histone 3 exhibited a typical priority distribution pattern (Fig. 2), with peak distances of around 150–200 bp. This pattern verifies that our ChIP procedure did not perform selective precipitations erroneously, thus this distribution pattern also indirectly validates our ChIP procedures.

The ChIP-seq chromatin data were then visualized using a local implementation of the UCSC Genome Browser (Karolchik et al. 2007). Figure 3a is a representative chromosomal region, demonstrating the type of coverage obtained by antibodies to total H3 or specific to acetyl-H3K9 and H3K27. While dynamic changes in genome-wide histone H3 lysine 9 (H3K9) and histone H3 lysine 27 (H3K27) acetylation patterns occur in response to 10 mM butyrate treatment, some sites on the highly enriched region of histone H3 are not changed (Fig. 3b). An enriched region present for all three ChIP-Seq data sets or stable binding sites may indicate certain chromatin structures that are tightly associated with histone.

Genomic-wide survey of the functional genomic distribution of H3, acetyl-H3K9, and acetyl-H3K27-enriched regions

To determine the location of H3, acetyl-H3K9, and acetyl-H3K27 binding sites within the bovine genome, we analyzed the histone 3, acetyl-H3K9, and acetyl-H3K27-

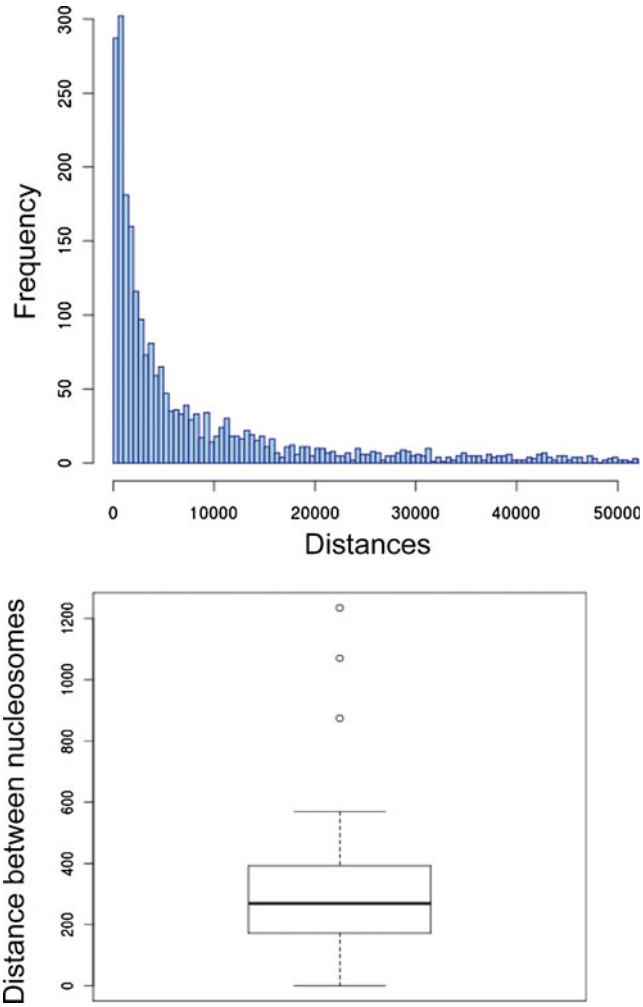

Fig. 2 *Up panel* ChIP-seq peak distribution (distance) of normal histone H3 in chromosome 1. *Lower panel* whole genome distribution of normal histone H3 ChIP-seq peaks

enriched binding regions in the proximal promoter (NDG analysis) within 5 kB upstream or at the 5′ untranscripted region (UTR) from the TSS, exon, and intron. This analysis is based on the location of the peak's central point of the peak region. Sometimes, the central point falls out of a known gene even though the peak itself overlaps the gene. In this case, the overlapping regions are defined as "intergenic" regions (Nelson et al. 2004). A detailed analysis of the genomic locations of the peaks of H3, acetyl-H3K9, and aceyl-H3K27 is shown in Table 2. Among the peaks that exhibited overlapping gene features, only about 3% to 5% of histone 3, acetyl-H3K9, and acetyl-H3K27 high-peak binding sites were located in intergenic regions, while the major portions of the peaks were located in the introns (88.1%, 85.6%, and 89.0%) and exons (4.6%, 6.1%, and 5.6%). This may represent the specific properties of these histones. Unlike some transcription factors, such as STAT6, which has 47% of its binding sites in intergenic regions

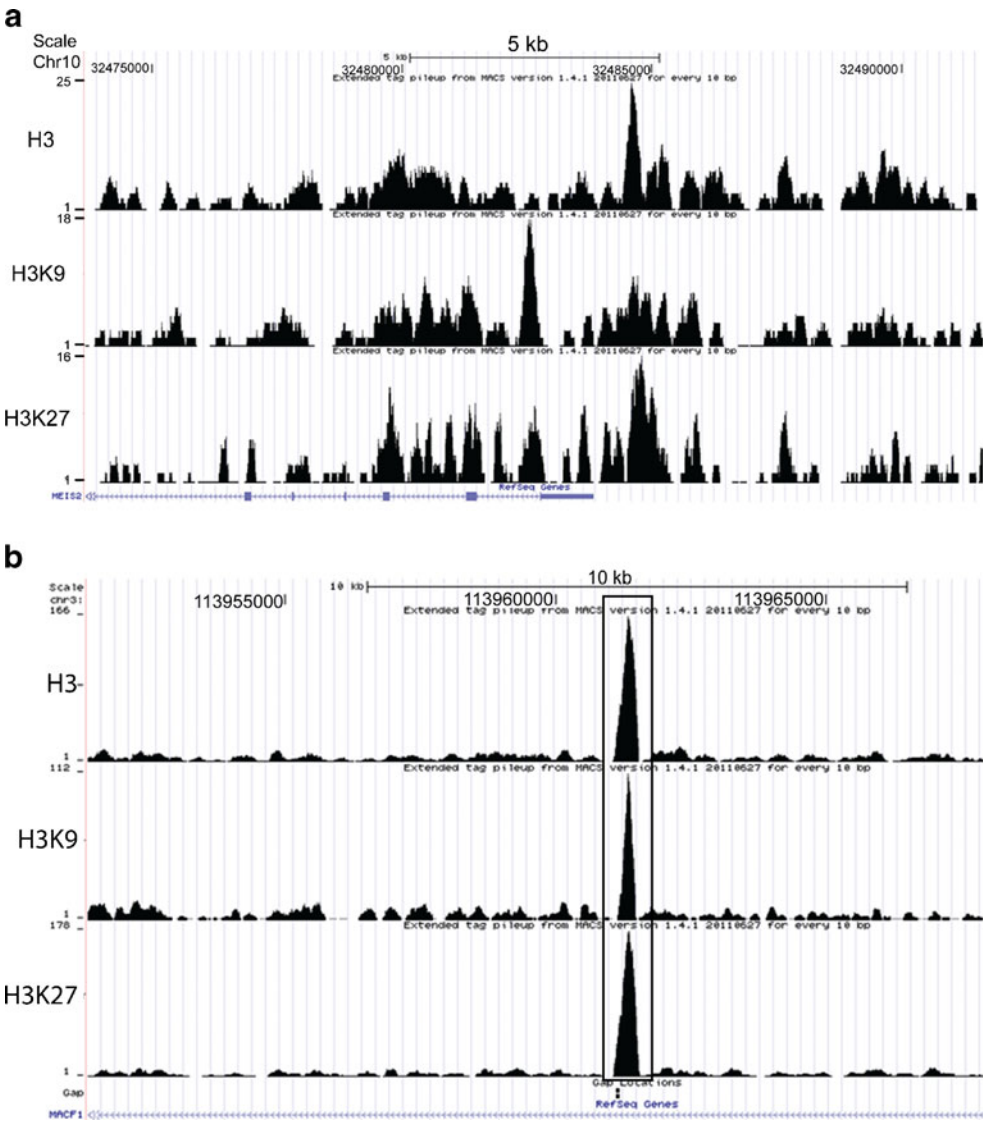

Fig. 3 UCSC browser view of genomic data of representative chromosome regions. The amount of sequence coverage for the different samples is shown to the left of each track (*y-axis*), which represents the number of times each region was recovered by the ChIP-seq. The tracks are total histone H3 from normal cells without butyrate treatment, acetyl-H3K9, and acetyl-H3K27 from butyrate-treated cells. Both *upper and lower panels* are from chromosome 10: representative regions of chromosome 10

(Tozawa et al. 2011), in our experiments, histone H3, acetyl-H3K9, and acetyl-H3K27 only have 5.2% (H3), 5.28% (acetyl-H3K9), and 3.2% (acetyl-H3K27) of their binding sites located in the intergenic regions, respectively. There are also about 9% of the high-peak binding sites of H3, acetyl-H3K9, and acetyl-H3K27 located 0–5 kb upstream from the nearest genes. These findings are summarized graphically Fig. 4a–c.

Table 2 The functional genomic distribution of H3, acetyl-H3K9, and H3K27-enriched regions

Column 1	H3 (%)	H3K9 (%)	H3K27 (%)
3′ UTR	0.80	1.04	0.88
Last intron	3.38	3.92	3.67
5′ UTR	1.27	1.97	1.18
Exons	4.62	6.11	5.63
Intergenic	5.20	5.28	3.20
First intron	28.74	32.73	27.01
Other introns	56.00	48.95	58.42

The distance from the TSS was also calculated between the peak's central points to the TSS of the nearest gene. Since the distance was calculated to the nearest TSS rather than the nearest downstream TSS, the value can be both positive and negative (Fig. 5a–c).

The distribution of histone H3, acetyl-H3K9, and acetyl-H3K27, correlated with transcription activity induced by butyrate

To expose the potential association between the enrichment of genome-wide histone H3, acetyl-H3K9, and acetyl-H3K27 and target gene transcription activities, we analyzed gene transcription activity and the association of the

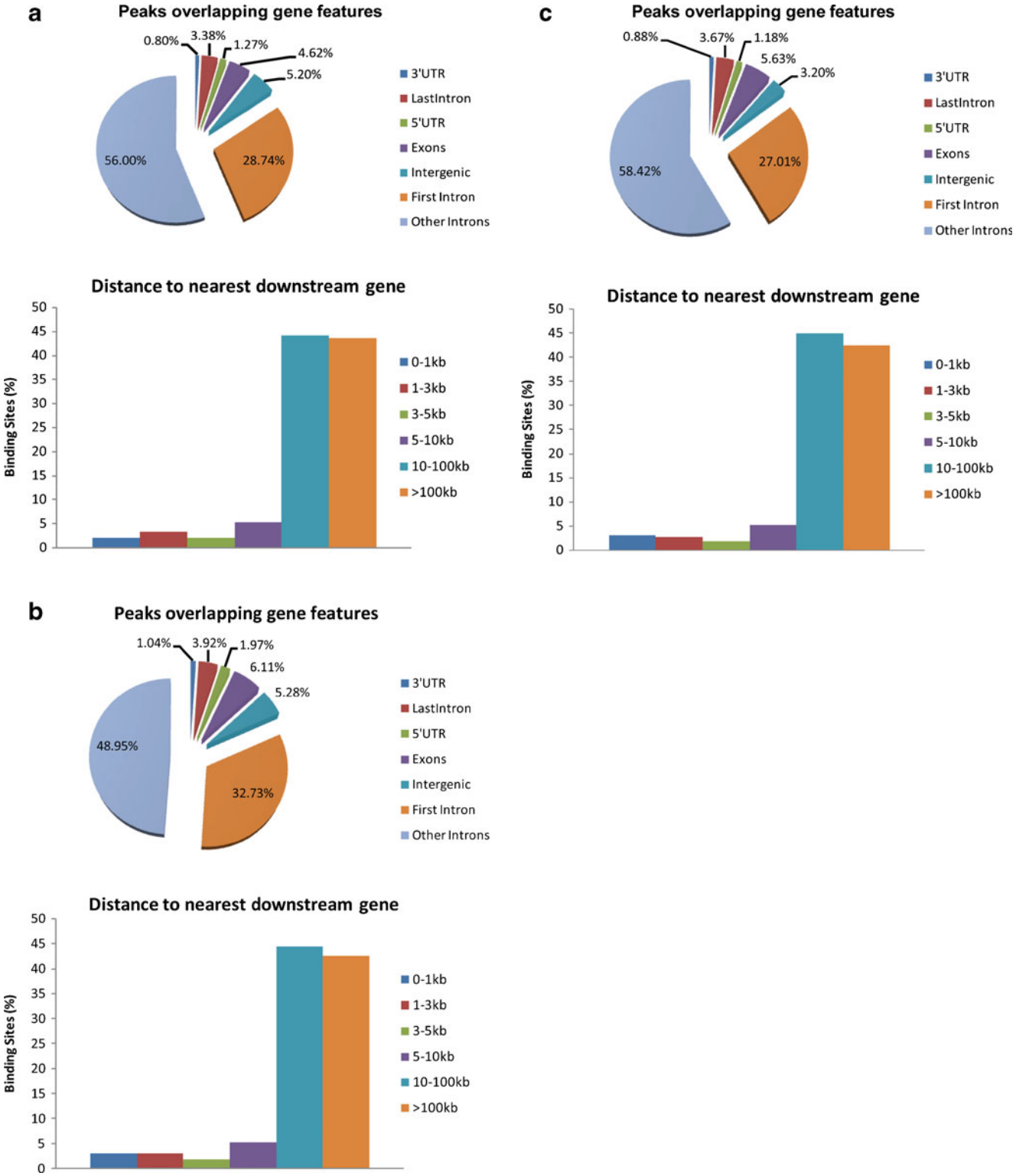

Fig. 4 Nearest downstream gene (*NDG*) analysis. The position of peaks within genes is plotted. This is plotted based on the location of the central point of the peak region in the proximal promoter at the 5′ untranscribed region (*UTR*) from the TSS, exon, intron, and intergenic region. **a** Distribution of histone H3 from the ChIP-seq of normal cells. **b** Distribution of acetyl-H3K9 enriched region from the ChIP-seq of butyrate-treated cells, and **c** acetyl-H3K27 enriched region from the ChIP-seq of butyrate-treated cells

acetylation of histone H3. The detailed analysis of the genomic locations of the peaks of H3, acetyl-H3K9, and acetyl-H3K27 in the gene ORC1L region are presented in Fig. 6 as visualized by the UCSC genomic browser view of

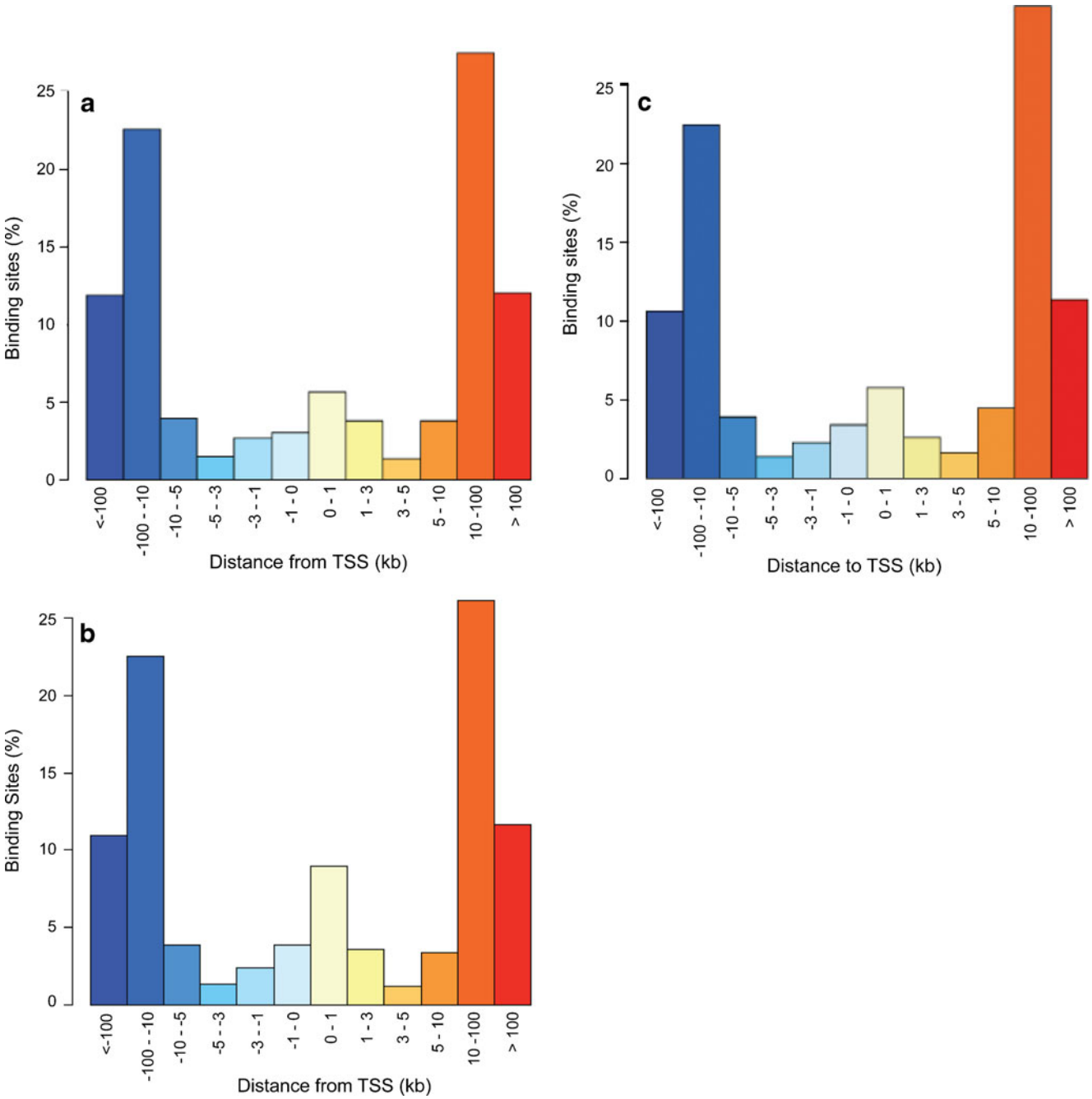

Fig. 5 Transcription start site (*TSS*) analysis. The distance is calculated between the central point of the peak to the TSS of the nearest gene. Since the distance in calculated to the nearest TSS rather than the nearest downstream TSS, the values can be both positive and negative. **a** Histone H3 from ChIP-seq of normal cells; **b** acetyl-H3K9-enriched region from the ChIP-seq of butyrate-treated cells; and **c** acetyl-H3K27-enriched region from the ChIP-seq of butyrate-treated cells

the region genomic data. The expression of ORC1L was downregulated by butyrate-induced histone acetylation, which was confirmed by both microarray experiments (Li et al. 2007) and a Western blot of protein (Li and Li 2008) in our laboratory. The sequence coverage of enrichments from the ChIP-seq of anti-H3, anti-acetyl-H3K9, and anti-acetyl-H3K27 indicates the binding shift of histone acetylation in the region induced by butyrate, especially immediately upstream (~2 kb) from the ORC1L gene.

We evaluated two different groupings of genes that have binding peaks detected by the ChIP-seq: (1) the ChIP-seq peaks overlapping the gene structure and (2) the ChIP-seq peaks located upstream from the genes. Among the 371 genes that were regulated by the butyrate-induced acetylation

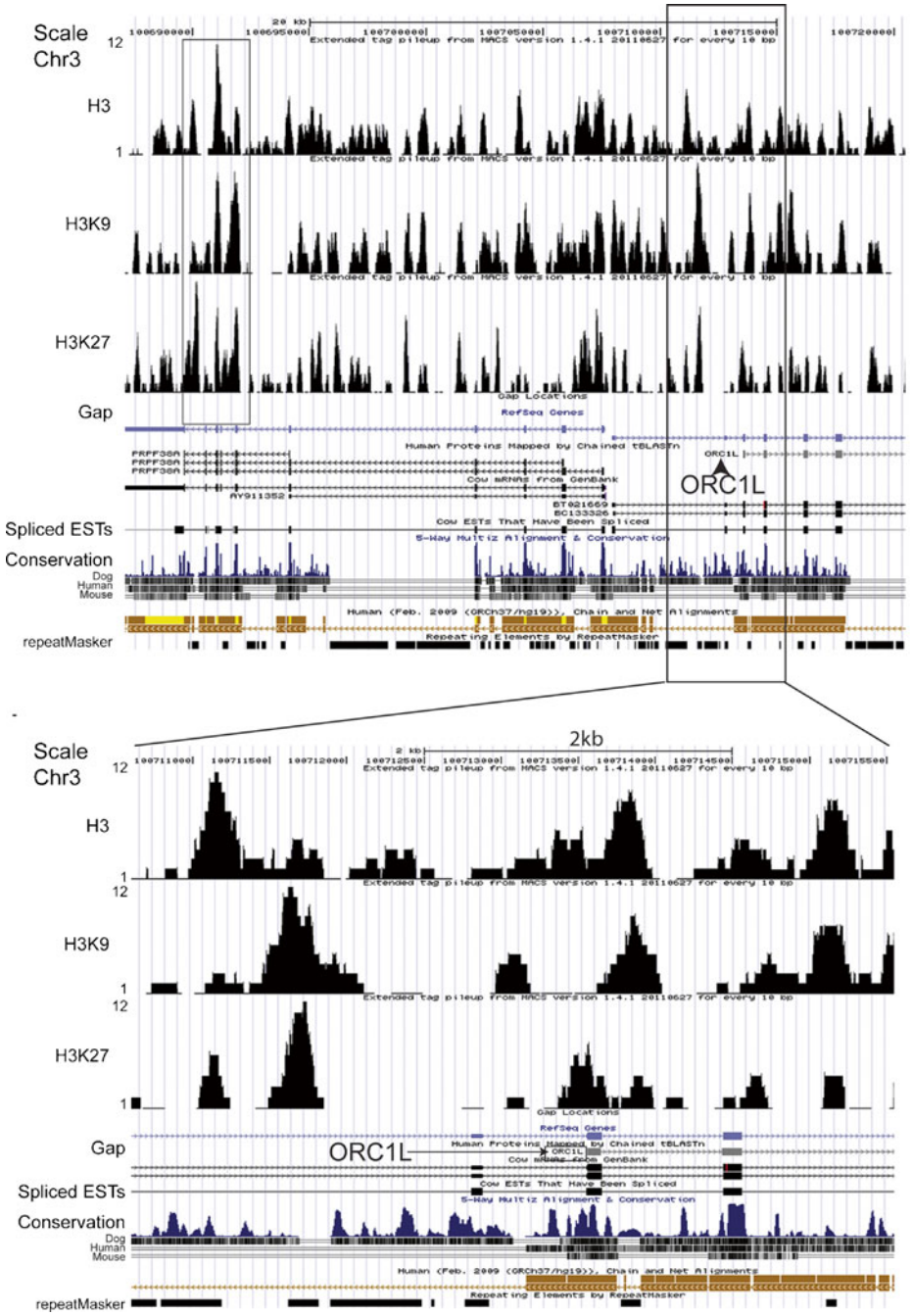

Fig. 6 UCSC browser view of genomic data of ORC1L gene region in chromosome 3 and an expanded of upstream region of ORC1L are shown. The amount of sequence coverage for the different samples is shown to the left of each track (*y-axis*), which represents the number of times each region was recovered by the ChIP-seq. The tracks are total histone H3 from normal cells without butyrate treatment, acetyl-H3K9, and acetyl-H3K27 from butyrate-treated cells

of histone, the ChIP-seq with anti-total H3 detected 44 genes (11/9%) with binding enrichment that overlapped the genes' structures. The ChIP-sep with anti-acetyl-H3K9 detected 31 genes (8.4%), and the ChIP-seq with anti-acetyl-H3K27 detected 81 genes (21.8%).

In most cases, there were multiple binding sites present on each of those genes. A total of 166 genes (42.1%) were associated with either histone H3 (Fig. 7) or acetyl-H3K9- and acetyl-H3K27-enriched binding sites located in the functional structures of the affected genes. In contrast, only 29 of 371 genes (7.8%) had ChIP-seq-detected enriched binding sites located upstream from the genes (11 genes with anti-histone H3; 4 genes with anti-acetyl-H3K9, and 14 genes with anti-acetyl-H3K27).

To determine the biologically relevant networks of the genes with ChIP-seq-detected enrichments with anti-H3 or acetyl-H3K9 and acetyl-H3K29 antibodies, as well as the potential association with the gene expression induced by butyrate, core analysis and comparison analysis were done with the Ingenuity Systems Pathway Analysis (IPA®). A merged network of butyrate-induced gene expression and ChIP-seq-detected binding sites from the genes detected by

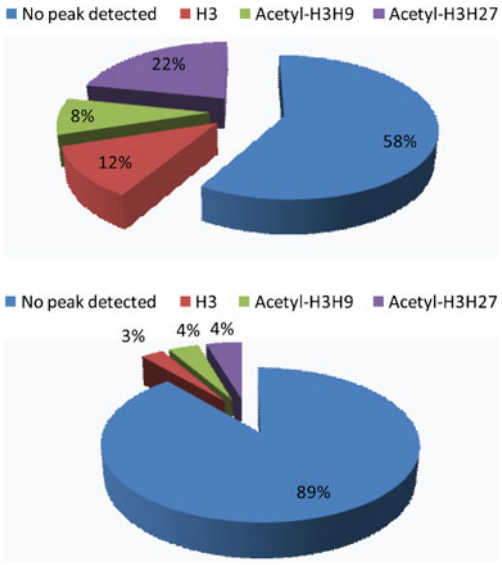

Fig. 7 Correlation of genes perturbed by butyrate treatment and ChIP-seq-detected binding peaks. Two different groupings of genes that have binding peaks detected by the ChIP-Seq: (1) ChIP-seq peaks overlapping the gene structure (*upper panel*) and (2) ChIP-seq peaks located upstream from the genes (*lower panel*)

anti-H3K27 ChIP-seq is presented in Fig. 8c. In the network, green indicates that gene expression was downregulated by butyrate and red indicates that gene expression was upregulated by butyrate. A selected group of genes (ORC1L, MCM3, MCM4, MCM5, and MCM6) and histone H3, H4 and HDAC9 were highlighted with a red circle because their interactions had been observed and reported in earlier publications (Li and Li 2006, 2008).

Motif discovery revealed different binding preferences among histone H3, acetyl-H3K9, and acetyl-H3K27

Using the GADEM algorithm, an efficient de novo motif discovery tool for large-scale genomic sequence data, several motifs were generated for each of the ChIP-seq datasets (Fig. 9a–c). A de novo search for H3, acetyl-H3K9, and acetyl-H3K27 binding motifs indicated that histone modification (acetylation) at different locations changes the sequence-based binding preference of histone H3. Figure 9a shows the multiple alignments of these 12 binding sites (4 binding sites from each of the three ChIP-seq data sets), with a consensus sequence of TCXTCTCGAGY (For convenience, a single base is shown if it occurs in more than half of the sites and at least twice as often as the second most frequent base. Otherwise, a degenerate symbol is used). Figure 9b, c shows two core motifs of TCACGTGGCT and GAGGCAGGAAA, with much higher conservation in the flanking bases.

Discussion

Chromatin modification has clearly emerged as a very critical mechanism in the regulation of the genome's transcriptional status (Goldberg et al. 2007). Butyrate-induced biological effects in bovine cells serve as an example of epigenetic regulation and provide a basis for understanding the full range of butyrate's potential biological roles and molecular mechanisms in animal cell growth, proliferation,

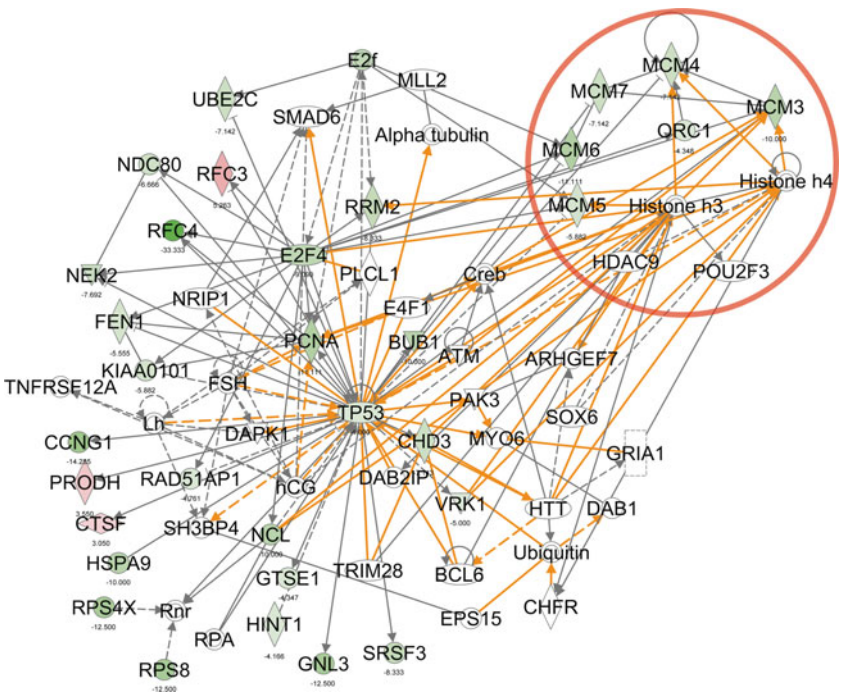

Fig. 8 A representative merged network of the genes perturbed by butyrate treatment and the genes have ChIP-seq-detected binding sites, in this case, from the genes detected by the anti-H3K27 ChIP-seq. In the network, *green* indicates that gene expression was downregulated by butyrate and *red* indicates that gene expression was upregulated by butyrate. A selected group of genes (ORC1L, MCM3, MCM4, MCM5 and MCM6) and histone H3, histone H4 and HDAC9 were highlighted

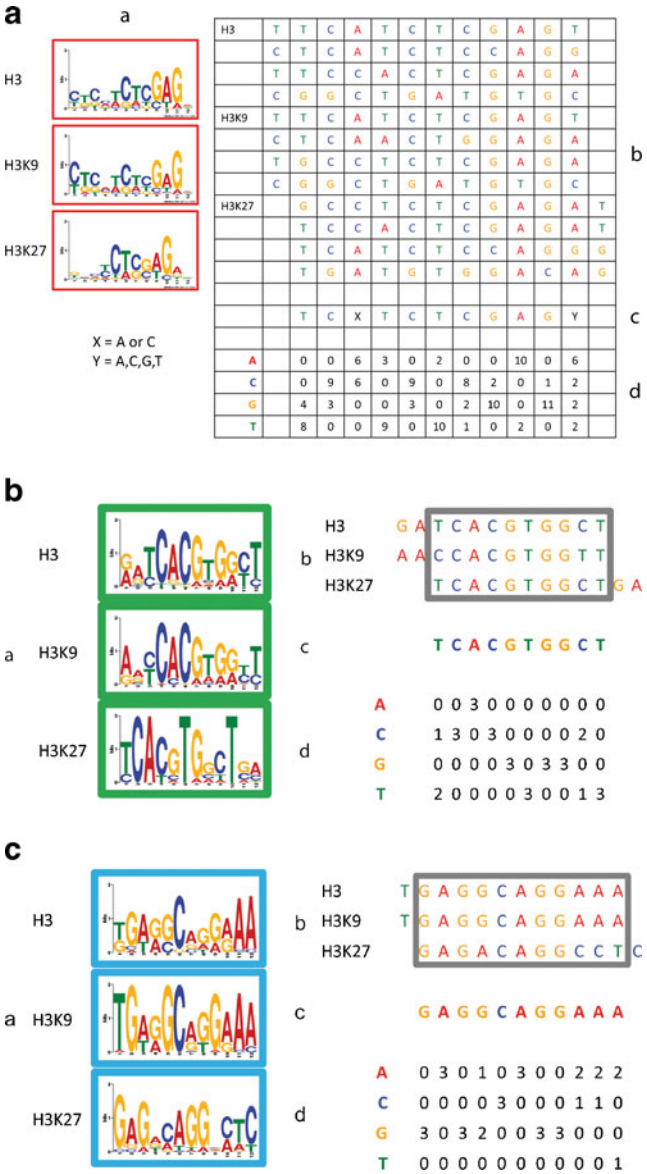

Fig. 9 Characterization of histone H3, acetyl-H3K9, and acetyl-H3K27 binding motifs. **a** A binding motif with a high degree of variation: sequence logo showing the frequencies scaled relative to the information content (measure of conservation) (*a*), 12 binding sites (4 binding sites from each of the three ChIP-seq data sets) (*b*), degenerate consensus sequence (*c*); frequencies of nucleotides at each position (*d*). **b**, **c** Two highly conservative motifs: sequence logo showing the frequencies scaled relative to the information content (measure of conservation) (*a*); three binding sites (from each of the three ChIP-seq data sets) (*b*); degenerate consensus sequence (*c*); frequencies of nucleotides at each position (*d*)

and energy metabolism. Experimental approaches to understanding the biology of histone acetylation have generally been oversimplified since researchers have mainly examined only one or two lysines, or a few genomic loci at a time. A comprehensive and high-resolution colocalization analysis of all histone acetylation for the entire bovine genome is required to understand the functional correlation among the various histone lysine acetylations in processes such as transcription and DNA replication. This study was designed to utilize next-generation sequencing technology, combined with ChIP technology to comprehensively, quantitatively, and cost-effectively analyze histone modification (acetylation) and to map protein target sites in the bovine genome that are responsive to modulation by butyrate.

We show that the peak distribution of the ChIP-seq reads for normal histone 3 exhibited a typical priority distribution pattern. The most important architectural genome elements are the basic repeats of nucleosomes in which DNA wraps histone proteins. Multiple histones wrap into a 30-nm filament consisting of nucleosome arrays. Depending on the state of the chromatin structure (euchromatin or heterochromatin), the structure of the 30-nm chromatin filament for DNA repeat-length per nucleosome ranges from 177 to 207 bp (Wong et al. 2007). Our ChIP-seq data are consistent with this characteristic genomic architecture. This distribution pattern validates our ChIP procedures indirectly and confirms that our ChIP procedure did not select precipitations erroneously. Our data also indicate that butyrate-induced histone acetylation can significantly modulate chromatin binding patterns. In addition to many dynamic changes of the histone H3 binding sites induced by butyrate, we also discovered that there are many H3 binding sites that are very stable. Those binding sites (enriched region) appear in all three ChIP-seq mappings. Those stable enriched regions presented in all three ChIP-seq data sets may indicate certain chromatin structures that are tightly associated with histone.

The enrichment of acetyl-histone to regions of DNA is not necessarily correlated with changes in gene expression. To expose the potential association between the target gene transcription activities and the enrichment of genome-wide histone H3, acetyl-H3K9, and acetyl-H3K27, and target gene transcription activities, we analyzed gene transcription activity and the association of the acetylation of histone H3. The expression of ORC1L was downregulated by butyrate-induced histone acetylation, which was confirmed in our laboratory by both microarray experiments (Li et al. 2007), RT-PCR, and a Western blot of protein (Li and Li 2008). Recent studies have indicated that acetyl-H3K27 is the mark of active regulatory regions, such as promoters and enhancers, in the mammalian genome (Zhou et al. 2011). We show here that the downregulation of ORC1L is accompanied by a shift of acetyl-H3K9 and acetyl-H3K27 at the transcriptional start site of ORC1L. The sequence coverage of enrichments from the ChIP-seq of anti-H3, anti-acetyl-H3K8, and anti-acetyl-H3K27 indicates the binding shift of histone acetylation in the region induced by butyrate, especially immediately upstream (~2 kb) from the ORC1L gene.

As a vital step towards comprehensive understanding of the molecular mechanism of butyrate-induced acetylation,

as well as its biological effects, we also utilized IPA® to explore the potential association between ChIP-seq data and butyrate-induced gene expression, based on our microarray experiments (Li et al. 2007). Because no database for the bovine gene expression is currently publically available, genes that were up- or downregulated at least 2.5-fold (<−2.5 or >2.5) and met a stringent median FDR cutoff of 0% were selected from our microarray experiments in which butyrate-exposed MDBK cells were compared to noninduced cells. Only genes that were homologous to their respective human counterparts and/or with known functions and pathways (371 genes, 285 down- and 86 upregulated genes) were approved by the HUGO Gene Nomenclature Committee, and the genes with binding sites detected by ChIP-seq were subjected to the IPA. With an integrative analysis of ChIP-seq and expression profiling data, very interestingly, we discovered that a total of 166 genes (42.1%) that are strongly regulated by butyrate-induced histone acetylation are associated with either histone H3 (Fig. 7) or acetyl-H3K9- and acetyl-H3K27-enriched binding sites located in the affected genes' functional structures. In contrast, only 29 of 371 genes (7.8%) have ChIP-seq-detected enriched binding sites located upstream from the genes (11 genes with anti-histone H3; 4 genes with anti-acetyl-H3K9 and 14 genes with anti-H3H27). In addition, a merged network of genes perturbed by butyrate treatment and genes have ChIP-seq-detected binding sites, in this case, from the genes detected by the anti-H3K27 ChIP-seq, indicates the functional association of butyrate-induced acetylation of H3K9 and H3K27 with the gene expression regulation induced by butyrate.

Our analysis of the consensus sequences bound to H3, acetyl-H3K9, and acetyl-H3K27 reveals several consensus sequences (motifs) from each of the ChIP-seq data sets. Sequence motifs are short, recurring patterns in DNA that are presumed to have a biological function (D'Haeseleer 2006). The motifs usually indicate sequence-specific binding sites for proteins such as nucleases and transcription factors, and in our case, one important chromatin component histone H3. Computational analysis of the ChIP-seq data makes it possible to derive genome-wide binding patterns for the histone H3 core, acetyl-H3K9, and acetyl-H3K27. Our results reveal that butyrate-induced acetylation of H3K9 and H3K27 changes the sequence-based binding preference of histone H3. The differences in the binding motifs for acetyl-H3K9 and acetyl-H3K27 indicate that histone modification (acetylation) at various lysine sites changes the histone H3 binding preferences, either independently or cooperatively. In either situation, it is evident that butyrate-induced acetylation of histone plays a role in changing chromatin structure and in defining genetic regulatory networks and interpreting the regulatory program of individual genes. In addition to the variation of the binding preferences of acetylated histone H3 as the results of acetylation, another interesting finding in our data is a high degree of conservation in histone binding also evidently presented in our data. This may present a key property of living systems of robustness, e.g., the ability to maintain phenotypic stability in the face of diverse perturbations arising from environmental changes (Stelling et al. 2004). Recent progress on our understanding of epigenetics at the molecular level is remarkable, however epigenetics is intimately related to robustness as both lie between genotypes and phenotypes (Ohta 2011). More understanding at the molecular level of robustness and epigenetics certainly is an urgent task.

It is unavoidable that there are some shortcomings in the data drawn from these in vitro experiments. Nevertheless, MDBK as an established bovine cell line with inducible gene expression regulatory events certainly is an ideal and invaluable tool for functional genomic studies. Together, our data provide supporting evidence that butyrate-induced histone acetylation may change the epigenomic landscape, therefore regulating the expression of genes. An integrated ChIP-seq analysis and gene expression profiling show that butyrate-induced acetylation of H3K9 and H3K27 changes the sequence-based binding preference of histone H3 and underlies the potential mechanisms of butyrate-induced gene expression regulation. Thus our data reveal that butyrate-induced acetylation of histone H3K9 and H3K27 plays a role in gene expression regulation and in the complicated and dynamic epigenomic landscape that is formed by a variety of histone modifications.

References

Bailey TL, Elkan C (1994) Fitting a mixture model by expectation maximization to discover motifs in biopolymers. Proceedings/… International Conference on Intelligent Systems for Molecular Biology; ISMB. International Conference on Intelligent Systems for Molecular Biology 2:28–36

Baldwin RL (1999) The proliferative actions of insulin, insulin-like growth factor-I, epidermal growth factor, butyrate and propionate on ruminal epithelial cells in vitro. Small Rumin Res 32:261–268

D'Haeseleer P (2006) What are DNA sequence motifs? Nat Biotechnol 24(4):423–425

Feng J, Liu T et al (2011) Using MACS to identify peaks from ChIP-Seq data. Curr Protoc Bioinformatics Chapter 2: Unit 2 14

Fischer A, Sananbenesi F et al (2007) Recovery of learning and memory is associated with chromatin remodelling. Nature 447 (7141):178–182

Goldberg AD, Allis CD et al (2007) Epigenetics: a landscape takes shape. Cell 128(4):635–638

Karolchik D, Hinrichs AS et al (2007) The UCSC Genome Browser. Curr Protoc Bioinformatics Chapter 1: Unit 1 4

Langmead B, Schatz MC et al (2009a) Searching for SNPs with cloud computing. Genome Biol 10(11):R134

Langmead B, Trapnell C et al (2009b) Ultrafast and memory-efficient alignment of short DNA sequences to the human genome. Genome Biol 10(3):R25

Li CJ, Elsasser TH (2005) Butyrate-induced apoptosis and cell cycle arrest in bovine kidney epithelial cells: involvement of caspase and proteasome pathways. J Anim Sci 83(1):89–97

Li RW, Li C (2006) Butyrate induces profound changes in gene expression related to multiple signal pathways in bovine kidney epithelial cells. BMC Genomics 7:234

Li RW, Li CJ (2007) Effects of butyrate on the expression of insulin-like growth factor binding proteins in bovine kidney epithelial cells. Open Vet Sci J 2007(1):14–19

Li CJ, Li RW (2008) Butyrate induced cell cycle arrest in bovine cells through targeting gene expression relevant to DNA replication apparatus. Gene Regul Syst Biol 2:113–123

Li CJ, Li RW et al (2007) Pathway analysis identifies perturbation of genetic networks induced by butyrate in a bovine kidney epithelial cell line. Funct Integr Genomics 7(3):193–205

Li C-J, Li RW et al (2010) MicroRNA (miRNA) expression is regulated by butyrate-induced epigenetic modulation of gene expression in bovine cells. Genet Epigenet 3:23–32

Mali P, Chou BK et al (2010) Butyrate greatly enhances derivation of human induced pluripotent stem cells by promoting epigenetic remodeling and the expression of pluripotency-associated genes. Stem Cells 28(4):713–720

Marinova Z, Leng Y et al (2010) Histone deacetylase inhibition alters histone methylation associated with heat shock protein 70 promoter modifications in astrocytes and neurons. Neuropharmacology 60(7–8):1109–1115

Myzak MC, Dashwood RH (2006) Histone deacetylases as targets for dietary cancer preventive agents: lessons learned with butyrate, diallyl disulfide, and sulforaphane. Curr Drug Targets 7(4):443–452

Nelson CE, Hersh BM et al (2004) The regulatory content of intergenic DNA shapes genome architecture. Genome Biol 5(4):R25

Ohta T (2011) Near-neutrality, robustness, and epigenetics. Genome Biol Evol 3:1034–1038

Riggs MG, Whittaker RG et al (1977) *n*-Butyrate causes histone modification in HeLa and Friend erythroleukaemia cells. Nature 268(5619):462–464

Salmon-Divon M, Dvinge H et al (2010) PeakAnalyzer: genome-wide annotation of chromatin binding and modification loci. BMC Bioinformatics 11:415

Stelling J, Sauer U et al (2004) Robustness of cellular functions. Cell 118(6):675–685

Tozawa H, Kanki Y et al (2011) Genome-wide approaches reveal functional interleukin-4-inducible STAT6 binding to the vascular cell adhesion molecule 1 promoter. Mol Cell Biol 31(11):2196–2209

Wolffe AP, Guschin D (2000) Review: chromatin structural features and targets that regulate transcription. J Struct Biol 129(2–3):102–122

Wong H, Victor JM et al (2007) An all-atom model of the chromatin fiber containing linker histones reveals a versatile structure tuned by the nucleosomal repeat length. PLoS One 2(9):e877

Zhang Y, Liu T et al (2008) Model-based analysis of ChIP-Seq (MACS). Genome Biol 9(9):R137

Zhou VW, Goren A et al (2011) Charting histone modifications and the functional organization of mammalian genomes. Nat Rev Genet 12(1):7–18